

Cite this article as: Xue Yong, Zheng Jie, Yan Zhaoming, et al. Microstructure and Mechanical Properties of AZ31 Magnesium Alloy Prepared by Cyclic Expansion-Extrusion with Asymmetrical Extrusion Cavity[J]. Rare Metal Materials and Engineering, 2021, 50(05): 1583-1589.

ARTICLE

# Microstructure and Mechanical Properties of AZ31 Magnesium Alloy Prepared by Cyclic Expansion-Extrusion with Asymmetrical Extrusion Cavity

Xue Yong, Zheng Jie, Yan Zhaoming, Xu Jian, Zhang Zhimin, Li Xubin, Yang Yongbiao, Wang Qiang

School of Materials Science and Engineering, North University of China, Taiyuan 030051, China

**Abstract:** Cyclic expansion-extrusion with an asymmetrical extrusion cavity (CEE-AEC) was performed on AZ31 magnesium alloy, and the effects of deformation passes on grain refinement, texture evolution, and mechanical properties were studied. The results show that during the CEE-AEC process, the continuous dynamic recrystallization (CDRX) and discontinuous dynamic recrystallization (DDRX) occur, and the average grain size reduces from 344  $\mu\text{m}$  to 11.7  $\mu\text{m}$ . The (0001) basal texture intensity gradually increases with the increase of processing passes. The existence of asymmetric cavities in CEE-AEC dies causes a great deflection of the basal texture. In addition, the mechanical properties of the alloy improve, and the tensile yield strength (TYS), ultimate tensile strength (UTS), and elongation (EL) are 109 MPa, 211 MPa, and 30.8%, respectively.

**Key words:** magnesium alloy; cyclic expansion-extrusion; microstructure; mechanical property

Magnesium (Mg) alloy with great potential has a wide application prospect in the automotive industry and electronic products due to its high specific stiffness, low density, and good recyclability<sup>[1-3]</sup>. However, Mg alloy has the hexagonal close-packed (hcp) structure, resulting in the fact that only the basal slip system can be easily activated at room temperature (RT), which leads to poor mechanical properties of the as-cast Mg alloy<sup>[4]</sup>.

The wide application of magnesium alloys is restricted to some extent due to its restricted room-temperature mechanical properties, especially ductility. Therefore, many researchers worked to improve the performance of Mg alloys by adjusting the processing technique<sup>[5-7]</sup>. Severe plastic deformation techniques such as equal channel angular extrusion (ECAP)<sup>[8-10]</sup>, accumulative rolling bonding (ARB)<sup>[11]</sup>, repetitive upsetting-extrusion (RUE)<sup>[12,13]</sup>, and cyclic expansion-extrusion (CEE)<sup>[14-19]</sup> are widely used as the methods to effectively improve the mechanical properties of Mg alloy. ECAP is commonly used because of its repeatability, grain refinement effect, and modification

of the crystal texture of Mg alloys. However, recent studies show that CEE process is better than ECAP process under the same degree of deformation<sup>[19]</sup>. In addition, many researchers are attracted by the introduction of shear deformation to obtain strain gradients for better mechanical properties during the traditional processes<sup>[20]</sup>. Xu<sup>[21,22]</sup> and Wang<sup>[23]</sup> et al refined the grains and improved the mechanical properties of magnesium alloys by introducing shear deformation during extrusion. Tu<sup>[24]</sup> and Song<sup>[25]</sup> et al introduced shear deformation into the ECAP process to deflect the (0001) basal texture, facilitating the operation of basal sliding system, and thereby improving the ductility of the alloy.

Based on the research background, the CEE process with an asymmetric cavity to introduce shear strain for improving the performance of Mg alloy was proposed, i.e., cyclic expansion-extrusion with an asymmetrical extrusion cavity (CEE-AEC). The effect of CEE-AEC on the microstructure and properties of rare earth-Mg (RE-Mg) alloys were studied in the previous research, and microstructure with an average grain size of 1.2

Received date: May 11, 2020

Foundation item: National Natural Science Foundation of China (51675492); Natural Science Foundation of Shanxi Province (201801D121106)

Corresponding author: Wang Qiang, Ph. D., Professor, School of Materials Science and Engineering, North University of China, Taiyuan 030051, P. R. China, E-mail: yongxue395@163.com

Copyright © 2021, Northwest Institute for Nonferrous Metal Research. Published by Science Press. All rights reserved.

$\mu\text{m}$  after 3 passes of CEE-AEC process was obtained, and it was found that the basal texture weakens with increasing the number of processing<sup>[26,27]</sup>. Due to the existence of long period stacking ordered (LPSO) structure in RE-Mg alloys, the dynamic recrystallization (DRX) mechanism and texture are greatly affected during processing.

In this research, in order to intuitively observe the DRX mechanism and texture change during CEE-AEC process, AZ31 Mg alloy was used to study the effect of CEE-AEC process on grain refinement and mechanical properties.

## 1 Experiment

The as-cast AZ31 Mg alloy (Al content 2.96wt%, Zn content 0.87wt%, Mg: bal.) with a length of 100 mm, a width of 50 mm, and a height of 200 mm was used in this study. The general description for three orthogonal directions in AZ31 alloy is as follows: ED is for the extrusion direction (height), TD is for the transverse direction (length), and ND is for the normal direction (width).

As-cast alloy samples were homogenized in an electric furnace at 673 K for 12 h. Then the homogenized billets were extruded using CEE dies for 1, 2 and 3 passes at 350, 320, and 280 °C, respectively. Step temperature processing was used to control the effect of grain refinement. And the processing schematic is shown in Fig. 1. The extrusion rate was set as 1 mm/s, and oil-based graphite was used to reduce the friction between the billet and mold. After each pass, the deformed billets were water-quenched to maintain the microstructure. After the final extrusion pass, the samples were air cooled.

The observed samples and tensile samples were machined from the center of the deformed billets, as demonstrated in Fig. 2. The microstructures of samples were observed by optical microscope (OM, Axio Observer A2m Carl Zeiss), and electron back-scattered diffraction (EBSD, Hitachi SU5000 FE-SEM). The samples for OM observation were ground by SiC papers (600#, 1000#, 2000#, 3000#, and 5000#) and mechanically polished, and then chemically etched by the solution of 1 g picric acid, 14 mL alcohol, 2 mL acetic acid and 2 mL distilled water. Before EBSD observation, the samples were mechanically polished, followed by electro-polishing at a volt-

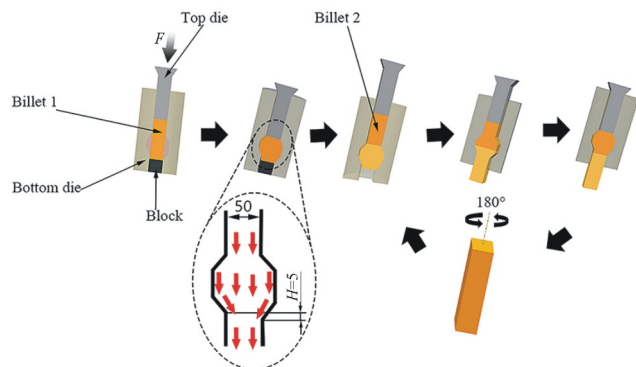


Fig.1 Schematic diagram of CEE-AEC process (unit: mm)

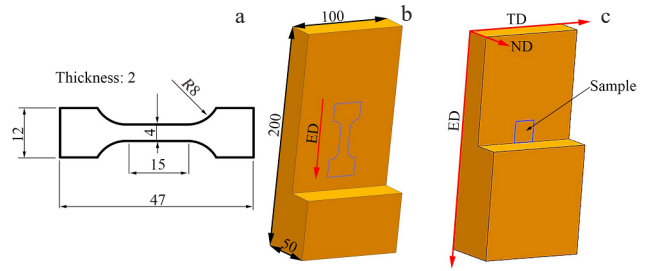


Fig.2 Dimensions of manufactured tension specimen (a); schematic diagrams of tension specimen (b) and observed sample of the billets (c) (unit: mm)

age of 15 V at  $-30\text{ }^{\circ}\text{C}$  for  $\sim 120\text{ s}$  with the perchloric acid-ethanol reagent (volume ratio is 1:9). The EBSD observation was performed on ED $\times$ TD plane of the samples, operating at 20 kV, tilt angle of  $70^{\circ}$  and working distance of 15 mm. The EBSD data were analyzed by orientation imaging microscopy (OIM) software to investigate the texture, grain size, etc. Tensile specimens were machined from the center of the deformed billets with tensile axis parallel to ED and the tensile tests were performed on 3382 Instron universal material experiment machine at RT with the strain rate of  $0.001\text{ s}^{-1}$ . To ensure the reliability of the experiments, each tensile test was performed three times and the mean value was used of three replicates for further analyses.

## 2 Results and Discussion

### 2.1 Microstructure of as-cast, homogenized and deformed AZ31 Mg alloys

Fig. 3 shows the microstructures of as-cast and homogenized AZ31 Mg alloys. The microstructure of as-cast alloy is shown in Fig. 3a, and the typical second phases  $\text{Mg}_{17}\text{Al}_{12}$  can be observed<sup>[28]</sup>. Fig. 3b and 3c demonstrate the microstructure of homogenized AZ31 Mg alloy. The average grain size is  $344\text{ }\mu\text{m}$ , and most of the second phases are basically incorporated into the Mg matrix. It is apparent from Fig. 4 that effective grain refinement is achieved after each pass of CEE-AEC process. As the number of processing passes increases, the number of coarse deformed grains decreases and the number of fine DRX grains increases. After the CEE-AEC process is completed, the samples are refined to  $11.7\text{ }\mu\text{m}$  (Fig. 4c). Fig. 5 summarizes the average grain size of AZ31 Mg alloy after each pass. After 1 pass, the average grain size is  $41.3\text{ }\mu\text{m}$ , and the deformed grains are surrounded by DRX grains (Fig. 4a), which is an obvious discontinuous dynamic recrystallization (DDR $X$ )<sup>[29]</sup>. As the cumulative strain increases, the number of deformed grains decreases after 2 passes of CEE-AEC process, with an average grain size of  $22.6\text{ }\mu\text{m}$ . Overall, after multi-pass CEE-AEC process, the average grain size decreases from  $344\text{ }\mu\text{m}$  to  $11.7\text{ }\mu\text{m}$ , and the grain refinement effect is very significant.

Fig. 6 shows the microstructure and texture of the deformed AZ31 Mg alloys by the orientation maps and pole figures. The



Fig.3 OM images (a, b) and EBSD inverse pole figure map (c) of as-cast (a) and homogenized (b, c) AZ31 Mg alloys

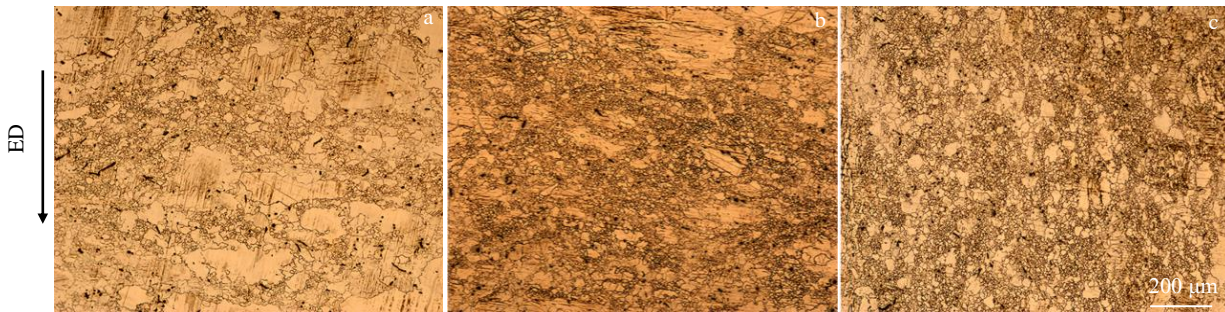


Fig.4 OM images of AZ31 Mg alloys after 1 pass (a), 2 passes (b), and 3 passes (c) of CEE-AEC process

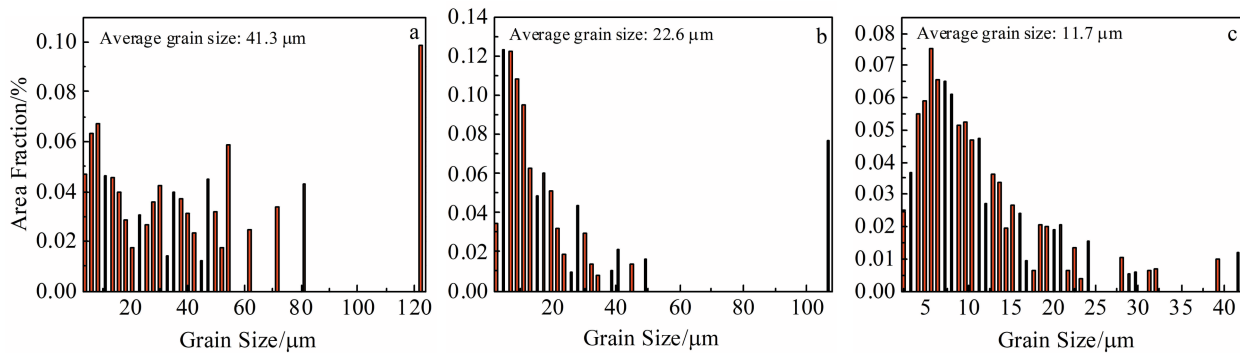


Fig.5 Average grain sizes of alloys after 1 pass (a), 2 passes (b), and 3 passes (c) of CEE-AEC process

low angle grain boundaries (LAGBs, misorientation angles between  $2^\circ$  and  $15^\circ$ ) are marked with the white lines and the high angle grain boundaries (HAGBs, misorientation angles higher than  $15^\circ$ ) are marked with the black lines, as demonstrated in Fig.6a~6c. Microstructure of the alloy after 1 pass of CEE-AEC is mostly heterogeneous with coarse and fine grains. Fig. 6a illustrates the typical bimodal microstructure, because the grain size statistics (Fig.5a) show a bimodal distribution composed of coarse grains of 50~120  $\mu\text{m}$  and fine grains  $<10 \mu\text{m}$ <sup>[29]</sup>. The coarse grains are surrounded by recrystallized grains, and the serrated grain boundary can be observed along the deformed grains. It can nucleate through the grain boundary bulging. The DDRX occurs during 1 pass of

CEE-AEC process, as shown by the white circles in Fig.6a<sup>[30]</sup>. In addition, fine grains can be seen inside the deformed grains (Fig.6a and 6b), which can be attributed to the transformation from LAGBs to HAGBs caused by the increase of cumulative strain, rather than the nucleation of DRX grains caused by the migration of grain boundary. This is a characteristic of typical continuous dynamic recrystallization (CDRX), as shown by the black circles in Fig.6a and 6b<sup>[31-33]</sup>. The (0001) and (10 $\bar{1}$ 0) texture of alloy after 1 pass of CEE-AEC process is relatively random and weakened, resulting in the fact that the maximum pole intensity of these two textures is 10.9 and 6.5, respectively (Fig.6a<sub>1</sub> and 6a<sub>2</sub>). The degree of grain refinement increases with increasing the strain. After 2 passes of CEE-AEC pro-

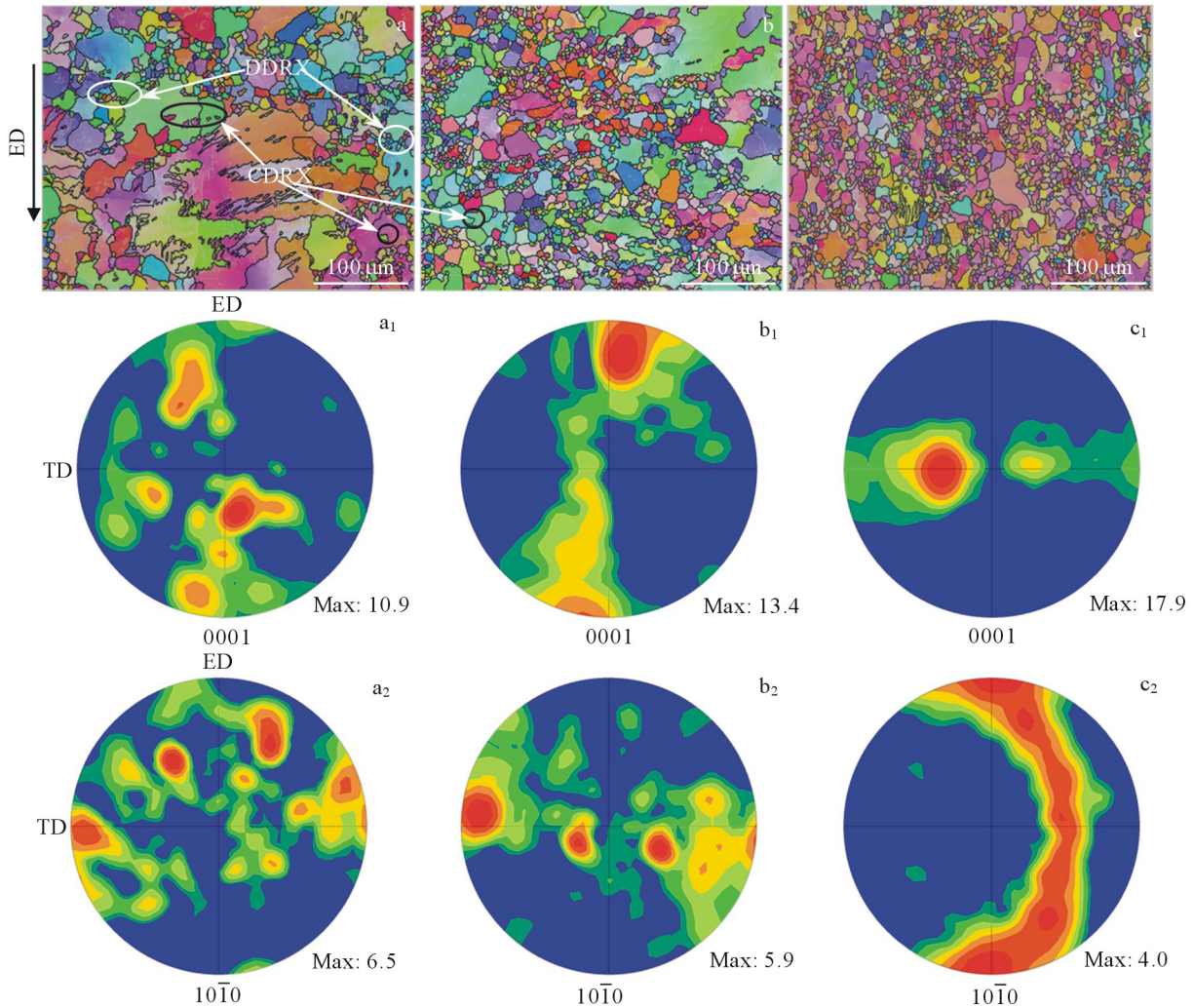


Fig.6 EBSD inverse pole figure maps (a~c) and (0001) (a<sub>1</sub>~c<sub>1</sub>) and (10 $\bar{1}$ 0) (a<sub>2</sub>~c<sub>2</sub>) pole figure maps of AZ31 Mg alloys after 1 pass (a, a<sub>1</sub>, a<sub>2</sub>), 2 passes (b, b<sub>1</sub>, b<sub>2</sub>), and 3 passes (c, c<sub>1</sub>, c<sub>2</sub>) of CEE-AEC process

cess, the coarse grains of the alloy are refined, and the typical bimodal microstructure is still visible (Fig.6b). Fig.6b<sub>1</sub> and 6b<sub>2</sub> reveal that the basal texture of the alloy after 2 passes of CEE-AEC process is enhanced with the maximum pole intensity of 13.4, but the maximum pole intensity of prismatic texture has a slight decrease. Fig.6c shows that grains are significantly refined after 3 passes of CEE-AEC process, and the microstructure of almost homogenous equiaxed grains appears. After 3 passes of CEE-AEC process, the maximum pole intensity of the basal texture increases to 17.9, and the maximum pole intensity of the prismatic texture decreases to 4.0 (Fig. 6c<sub>1</sub> and 6c<sub>2</sub>). In general, as the processing passes increases, the grains are gradually refined, and the pole intensity of the basal and prismatic textures increases and decreases, respectively. In addition, after 1 pass of CEE-AEC process, the basal texture with maximum pole intensity is tilted away from the ND by approximately  $\pm 30^\circ$  towards ED. After 2 passes of CEE-AEC process, the basal texture with the maximum pole intensity is tilted from the ND to the ED by approximately  $\pm 70^\circ$ . However, after 3 passes of CEE-AEC process, the basal texture with

the maximum pole intensity is tilted from the ND to TD by approximately  $\pm 45^\circ$ . The CEE-AEC process has a significant effect on grain refinement, and the presence of asymmetric cavities in the CEE-AEC mold has a significant effect on the texture rotation.

The Schmid factor (SF) for (0001)  $\langle 11\bar{2}0 \rangle$  basal slip of deformed billets in the center zone loading along ED is depicted in Fig.7. The SF value gradually decreases during the deformation process, but the reduction is very slight, and the average SF value of each pass is higher than 0.3. It is generally known that the basal slip is the predominant mode of deformation at room temperature<sup>[34]</sup>. When the external force is the same, the grains with larger SF value need smaller critical resolved shear stress (CRSS) to slip. Therefore, higher SF means the lower CRSS for basal slip<sup>[35]</sup>. In this research, compared with the status of alloys after 2 and 3 passes of CEE-AEC process, basal slip is easier to occur in the alloy after 1 pass of CEE-AEC process. When the tension is along the ED, many grains have (0001)  $\langle 11\bar{2}0 \rangle$  basal slip initiation with higher SF value.

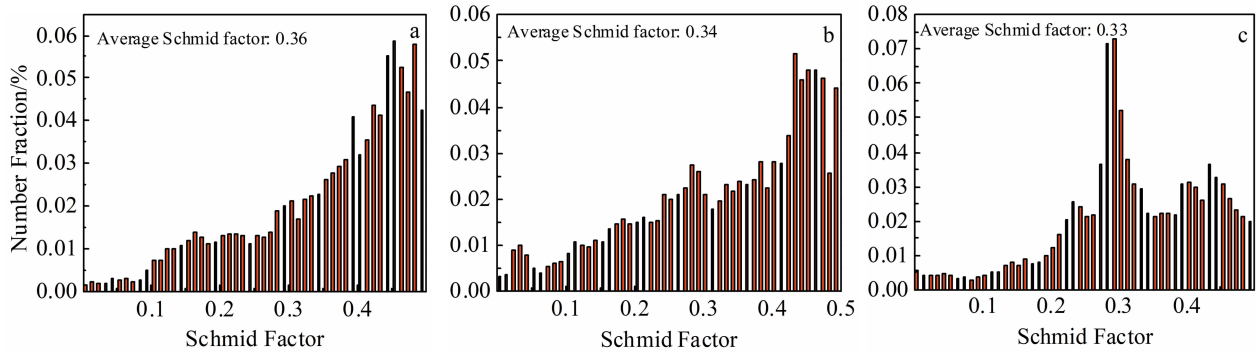


Fig.7 (0001) <1120> Schmid factor loading along ED of samples after 1 pass (a), 2 passes (b), and 3 passes (c) of CEE-AEC process

**2.2 Mechanical properties**

The tensile properties of each pass are shown in Fig.8. With increasing the deformation passes, the mechanical properties of the deformed alloy improve. Table 1 shows the corresponding values of specific tensile yield strength (TYS), ultimate tensile strength (UTS), and elongation (EL) of alloys after each pass of CEE-AEC process. The strengthening of comprehensive mechanical properties can be attributed to two aspects: the grain refinement and the texture. On one hand, the high strength in AZ31 Mg alloy is caused by grain refinement, which increases the impeditive effect on dislocation motion

**Table 1 Tensile yield strength (TYS), ultimate tensile strength (UTS), elongation (EL) of the deformed alloys**

Number of passes	TYS/MPa	UTS/MPa	EL/%
1	75	190	22.3
2	101	200	25.9
3	109	211	30.8

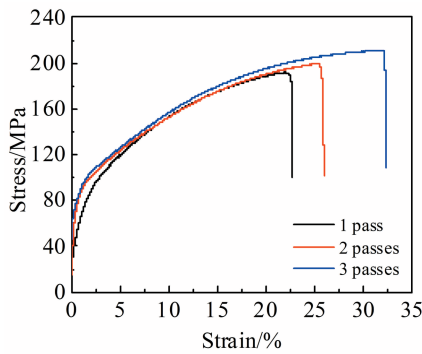


Fig.8 Stress-strain curves of CEE-AEC processed samples at room temperature

during plastic deformation<sup>[35]</sup>. The average grain size decreases from 41.3 μm (1 pass) to 22.6 μm (2 passes), which improves the TYS and EL of the 2-passes-deformed alloy. On the other hand, the increase of pole density of basal texture increases the TYS and UTS. Due to the existence of asymmetric cavities, the texture deflects after each pass. Although the intensity of the texture pole density increases, the SF value is basically the same and high, which results in the little change in the CRSS of the base slip. Therefore, the texture has little effect on the EL of alloys after 2 passes of CEE-AEC process. In general, as the number of processing pass increases, the comprehensive mechanical properties of the deformed alloy improve. After 3 passes of CEE-ACE, TYS, UTS and EL increase to 109 MPa, 211 MPa, 30.8%, respectively. Due to the existence of asymmetric cavities in the CEE-AEC dies, the basal texture of the deformed alloys after each pass severely deflects, and the effect of basal texture intensity on the EL weakens, so the SF value remains high value.

Fig.9 illustrates the fracture morphologies of the deformed

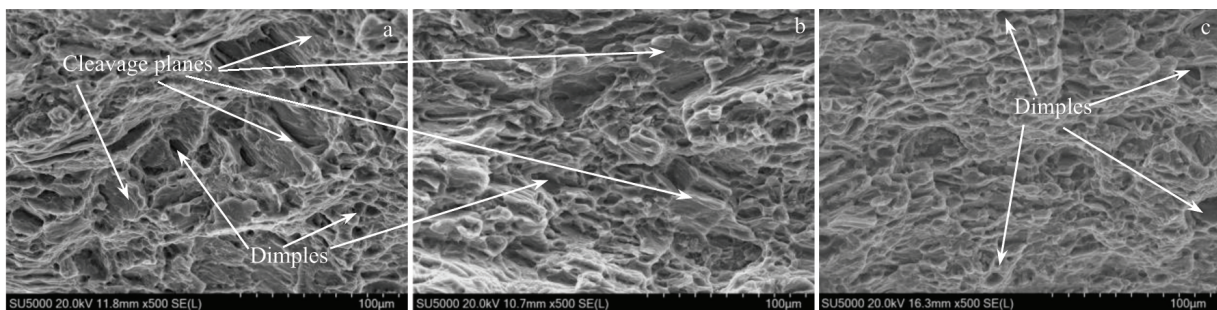


Fig.9 Fracture morphologies of samples after 1 pass (a), 2 passes (b), and 3 passes (c) of CEE-AEC process

alloys. As shown in Fig. 9a, many cleavage steps and a small number of dimples exist in the fracture morphology of alloy after 1 pass of CEE-AEC process. Then with the refinement of the grains, the recrystallized grains increases, and the ductility increases. After 2 passes of CEE-AEC process, the cleavage steps in the fracture morphology decrease, and the dimples increase. The large number of dimples in the fracture morphology of alloy after 3 passes of the CEE-AEC process indicates that the ductility greatly improves.

### 3 Conclusions

1) After 3 passes of cyclic expansion-extrusion with an asymmetrical extrusion cavity (CEE-AEC), the average grain size of AZ31 deformed alloy is refined from 344  $\mu\text{m}$  to 11.7  $\mu\text{m}$ , and the tensile yield strength (TYS), ultimate tensile strength (UTS) and elongation (EL) increase to 109 MPa, 211 MPa, 30.8%, respectively.

2) With increasing the processing passes, the basal texture intensity gradually increases, while the prismatic texture intensity gradually decreases. The maximum pole intensity of the basal texture increased from 10.9 (1 pass) to 17.9 (3 passes), and the maximum pole intensity of the prismatic texture decreases from 6.5 (1 pass) to 4.0 (3 passes). And the basal texture deflects greatly in each pass.

3) The existence of asymmetric cavities in the CEE-AEC process causes extra shear deformation during processing, which significantly deflects the basal texture of AZ31 alloy, leading to the fact that the Schmid factor (SF) of the basal slip is at a high level ( $>0.3$ ), although SF slowly decreases. In other words, the existence of the asymmetric cavity deflects the basal texture, reduces the influence of the texture on the ductility, and improves the comprehensive mechanical properties of the deformed AZ31 Mg alloys.

### References

- Zeng Z, Stanford N, Davies C H J et al. *International Materials Reviews*[J], 2018, 64(1): 27
- You S H, Huang Y D, Kainer K U et al. *Journal of Magnesium and Alloys*[J], 2017, 5(3): 239
- Agnew S, Nie J. *Scripta Materialia*[J], 2010, 63(7): 671
- Mirzadeh H. *Mechanics of Materials*[J], 2014, 77: 80
- Guo W, Wang Q, Ye B et al. *Journal of Alloys and Compounds* [J], 2013, 558: 164
- Dogan E, Vaughan M W, Wang S J et al. *Acta Materialia*[J], 2015, 89: 408
- Gong M, Xu S, Jiang Y et al. *Acta Materialia*[J], 2018, 159: 65
- Suh J, Victoria-Hernández J, Letzig D et al. *Materials Science and Engineering A*[J], 2016, 669: 159
- Sunil B R, Kumar T S S, Chakkingal U et al. *Materials Science and Engineering C*[J], 2016, 59: 356
- Victoria-Hernández J, Suh J, Yi S et al. *Materials Characterization*[J], 2016, 113: 98
- Rao X, Wu Y, Pei X et al. *Materials Science and Engineering A* [J], 2019, 754: 112
- Zhang G S, Meng Y Z, Yan F F et al. *Journal of Alloys and Compounds*[J], 2020, 815: 152 452
- Guo W, Wang Q D, Ye B et al. *Materials Science and Engineering A*[J], 2012, 540: 115
- Pardis N, Talebanpour B, Ebrahimi R et al. *Materials Science and Engineering A*[J], 2011, 528(25-26): 7537
- Pardis N, Chen C, Shahbaz M et al. *Materials Science and Engineering A*[J], 2014, 613: 357
- Pardis N, Chen C, Ebrahimi R et al. *Materials Science and Engineering A*[J], 2015, 628: 423
- Amani S, Faraji G, Abrinia K. *Journal of Manufacturing Processes*[J], 2017, 28: 197
- Amani S, Faraji G. *International Journal of Minerals, Metallurgy, and Materials*[J], 2018, 25(6): 672
- Xue Y, Chen S, Liu H et al. *Advances in Materials Science and Engineering*[J], 2019, 2019: 3 268 276
- Liu X Y, Lu L W, Sheng K et al. *Acta Metallurgica Sinica (English Letters)*[J], 2019, 32(6): 710
- Xu J, Jiang B, Song J et al. *Materials Science and Engineering A* [J], 2018, 732: 1
- Xu J, Yang T H, Jiang B et al. *Journal of Alloys and Compounds* [J], 2018, 762: 719
- Wang Q, Song J, Jiang B et al. *Materials Science and Engineering A*[J], 2018, 720: 85
- Tu J, Zhou T, Liu L et al. *Journal of Alloys and Compounds*[J], 2018, 768: 598
- Song D H, Zhou T, Tu J et al. *Journal of Materials Processing Technology*[J], 2018, 259: 380
- Yan Z M, Zhang Z M, Li X B et al. *Journal of Alloys and Compounds*[J], 2020, 822: 153 698
- Zheng J, Yan Z M, Yu J M et al. *Materials Research Express*[J], 2019, 6(10): 1065
- Zhao F, Suo T, Chen B et al. *Journal of Alloys and Compounds* [J], 2019, 798: 350
- Zhang H, Wang H Y, Wang J G et al. *Journal of Alloys and Compounds*[J], 2019, 780: 312
- Ghorbani A, Zarei-Hanzaki A, Nezhadfar P D et al. *The International Journal of Advanced Manufacturing Technology*[J], 2019, 102(5): 2307
- Zhou X, Liu C, Gao Y et al. *Metall Mater Trans A*[J], 2017, 48(6): 3060
- Li B, Teng B G, Chen G X. *Materials Science and Engineering A* [J], 2019, 744: 396
- Zhou G W, Li Z H, Li D Y et al. *Materials Science and Engineering A*[J], 2018, 730: 438
- Hutchinson W B, Barnett M R. *Scripta Materialia*[J], 2010, 63(7): 737
- Wang Y P, Li F, Shi W Y et al. *Materials Characterization*[J], 2019, 155: 109 842

## 差速循环扩挤制备的AZ31镁合金的组织 and 力学性能

薛 勇, 郑 杰, 闫钊鸣, 徐 健, 张治民, 李旭斌, 杨勇彪, 王 强  
(中北大学 材料科学与工程学院, 山西 太原 030051)

**摘 要:** 对AZ31镁合金进行了差速循环扩挤(CEE-AEC), 研究了变形道次对晶粒细化、织构演变和力学性能的影响。结果表明, 在差速循环扩挤过程中, 发生了连续动态再结晶(CDRX)和非连续动态再结晶(DDRX), 平均晶粒尺寸从344  $\mu\text{m}$ 减小到11.7  $\mu\text{m}$ 。随着加工道次的增加, (0001)基面织构强度逐渐增加。差速循环扩挤模具中不对称型腔的存在极大地引起了基面织构的偏转。此外, 合金的机械性能得到改善, 并且屈服强度(TYS)、抗拉强度(UTS)和断裂伸长率(EL)分别为109 MPa, 211 MPa和30.8%。

**关键词:** 镁合金; 循环扩挤; 微观结构; 机械性能

---

作者简介: 薛 勇, 男, 博士, 教授, 中北大学材料科学与工程学院, 山西 太原 030051, E-mail: yongxue395@163.com